Aqueous Ammonium-ion Hybrid Supercapacitors

Juguo Dai[a,b], Yizhang Yang[b], Jing Yu[a,c], Hucheng Fu[b], Yiting Xu*[,b], Qiaoyun Qin[d], Xueqiang Qi*[,a,d], Lizong Dai*[,b], Andreu Cabot*[,a,e]

a. Catalonia Institute for Energy Research (IREC), Sant Adrià de Besòs, 08930 Barcelona, Catalonia, Spain

b. Fujian Provincial Key Laboratory of Fire Retardant Materials, College of Materials, Xiamen University, Xiamen, 361005, China

c. Catalan Institute of Nanoscience and Nanotechnology (ICN2), CSIC and BIST, Campus UAB, Bellaterra 08193, Barcelona, Spain

d. College of Chemistry and Chemical Engineering, Chongqing University of Technology, Chongqing 400054, China.

e. ICREA, Pg. Lluis Companys 23, 08010 Barcelona, Catalonia, Spain

* Corresponding author email:

xyting@xmu.edu.cn, xqqi@cqut.edu.cn, lzdai@xmu.edu.cn, acabot@irec.cat

Abstract

Aqueous ammonium ion supercapacitors have garnered significant attention in recent years owing to their exceptional performance, environmentally sustainable, and safe nature, as well as their potential for cost-effectiveness. Despite notable progress in developing this technology, several challenges remain. These include identifying electrode materials with high specific capacity, comprehensively understanding the intercalation mechanism of ammonium ions, and clarifying how these ions interact with the electrode materials. This review article provides a comprehensive examination of the latest developments in the field, including aspects such as electrolyte composition, mechanisms of ammonium ion insertion, and advancements in electrode materials. Additionally, we offer insights into potential solutions to overcome the current limitations faced by ammonium ion supercapacitors, paving the way for further innovation and application of this promising technology.

Keywords: Ammonium, supercapacitor, hydrogen bonds, aqueous electrolyte, energy storage.

1. Introduction

Energy storage devices have become essential in various facets of daily life. With the growing adoption of electric vehicles and the increasing reliance on intermittent renewable energy sources such as solar and wind, the demand for cost-effective and safe energy storage solutions offering suitable energy density, fast charging, and long service life has become even more urgent. In response, extensive research and optimization over the past few decades have focused on key components such as electrode materials, charge carriers, electrolyte composition, and the electrolyte/electrode interphase.[1-15] Despite these efforts, current batteries, particularly lithium-ion batteries, still face several inherent challenges, including slow charging rates, risks of thermal runaway, moderate power densities, and the requirement for specific charging and operational conditions.[16-18]

Supercapacitors effectively complement batteries by addressing some of their key limitations, such as slow charging rates and low power outputs. Supercapacitors fall into two primary categories: 1) Electric-double-layer (EDL) supercapacitors are based on high surface area carbon materials, whose charge storage relies on the physically adsorbed ions at the electrodes-electrolyte interfaces. EDL supercapacitors rely solely on electrostatic interaction without undergoing Faradic reactions.[19-24] 2) Pseudo-capacitance supercapacitors are based on metal compounds, MXenes, metal-organic frameworks, covalent organic frameworks, organic molecular materials, and/or conductive polymers (MnO_2, MoS_2, MoO_3, polyaniline, COFs, MOFs, $Ti_3C_2T_x$ etc.) where charge storage is achieved through reversible redox reactions on or near the electrode surface.[25-30] In between, hybrid supercapacitors that combine these technologies are also being developed. These typically feature a pseudo-capacitive material at the cathode and an EDL material at the anode, aiming to blend the advantages of both types to enhance overall performance.

In addition to the electrode material, the physicochemical properties of charge carriers and their charge storage mechanisms critically influence the performance of supercapacitors. The most common carriers in supercapacitors and hybrid supercapacitors are metallic cations, such as lithium (Li^+), sodium (Na^+), potassium (K^+), zinc (Zn^{2+}), calcium (Ca^{2+}), magnesium (Mg^{2+}) and aluminum (Al^{3+}).[31-42] Among these, only Li^+ has been used in large-scale systems, with related

difficulties in terms of cost, secure supply, and safety. As an alternative, Zn^{2+} offers notable energy densities but its cost remains relatively high.[43-45] Beyond metallic ions, some non-metal charge carriers such as H^+ and OH^- are also used in supercapacitors. However, high concentrations of these ions put the electrode into harsh working conditions, limiting their service time.[29, 46-50]

Recently, ammonium ions have emerged as a viable non-metallic charge carrier alternative in batteries and supercapacitors.[51-55] Compared to metal cations, ammonium ions offer several advantages, including inherent safety, abundance, low molar mass (18 g mol^{-1}), and a small hydrated radius (3.31 Å).[56-59] Besides, NH_4^+ offers a milder electrolyte environment than H^+ and OH^-, and its ability to form hydrogen bonds with host materials can enhance the electrochemical capacity and especially the stability of energy storage devices. Despite these advantages, the development of NH_4^+-based batteries and supercapacitors lags significantly behind other electrochemical energy storage technologies.

To date, most previous reviews on ammonium ion energy storage have focused on batteries, discussing their working mechanisms and electrode materials involved,[53, 60] which differ significantly from those of supercapacitors.[61] In contrast, our review centers on ammonium ion supercapacitors, examining the role of charge carriers and introducing a new perspective on the impact of desolvation energy on their performance. We aim to advance the development of this promising technology by providing a comprehensive overview of recent progress in the field. We begin by explaining the working principles of aqueous NH_4^+-based supercapacitors, contrasting them with other energy storage systems. Next, we explore the mechanisms by which charge carriers interact with electrode materials, an understanding crucial for the design and engineering of high-performance electrodes, which is the focus of the following section. Finally, we present a current perspective on the state of the art, highlighting the existing challenges and proposing potential solutions to move the field forward.

2. Electrolyte and energy storage mechanisms

2.1 Charge carrier ions

Among the various charge carriers used in supercapacitors, hydrogen (H^+) stands out as a

non-metallic cationic charge carrier with the lowest ionic weight and smallest hydrated radius, potentially offering the fastest kinetics. The ionic conductivity of H^+ (350.1 S cm^2 mol^{-1}) surpasses that of most metallic cations and non-metallic anions, making it advantageous for achieving the desired electrochemical capacity in supercapacitors. However, a fundamental limitation of H^+-based aqueous electrolytes is the occurrence of hydrogen evolution when the working potential window exceeds the relatively low electrolysis potential (1.23 V). This narrow potential window significantly restricts the energy density ($E = 1/2CV^2$) of H^+(aq)-based supercapacitors.[62-64] To mitigate the hydrogen evolution reaction (HER), the concentration of H^+ in the solution must be reduced, which in turn decreases the capacitance (C). Another drawback of H^+-based supercapacitors is the insertion of H^+ as a much larger and heavier solvated species.[65-67] The most likely solvation structure for H^+(aq) is a distorted Eigen-type complex ($H_9O_4^+$), which results in a higher desolvation energy (11.66 eV).[68] The solvation sheath restricts the interaction of hydrogen ions with electrode materials, preventing the formation of hydrogen bonds, which can result in instability and contribute to significant self-discharge rates. Additionally, the corrosive nature of acidic electrolytes, such as H_2SO_4, poses significant challenges in designing cells that can achieve long-term stability.

On the other hand, OH^- anions have a low hydrated radius (3.00 Å), and high ionic conductivity (198 S cm^2 mol^{-1}).[69] When used in carbon-based supercapacitors, OH^- typically provides moderate specific capacitance with excellent cycling stability. However, like H^+, OH^- electrolytes suffer from a limited working potential window, where exceeding the electrolysis potential leads to oxygen evolution. Furthermore, alkaline electrolytes (e.g., KOH, NaOH) present similar corrosion challenges to those posed by acidic electrolytes, complicating cell design and longevity.

In contrast, metallic ions (Li^+, Na^+, K^+, Zn^{2+}, Ca^{2+}, Mg^{2+}, Al^{3+}, etc.) do not pose corrosion issues and can operate over larger potential windows. However, they face other challenges. As shown in Figure 1a, most metal ions are characterized by a relatively large ionic weight and hydrated radius, which result in slow reaction kinetics and low mobilities.[70]

A key factor in the charge/discharge process of supercapacitors is the insertion and deinsertion of charge carrier ions into electrode materials. For cation insertion, de-solvation—removing the hydration sheath surrounding the ion—is often an energy-intensive step that

becomes limiting for ions with large hydrated radii. Metallic ions generally require less energy for de-solvation compared to H^+. For example, the de-solvation energies for K^+ (4.12 eV) and Na^+ (4.76 eV) are significantly lower than for H^+ (11.66 eV). This suggests that bare metallic ions can more easily be inserted into electrode materials. While de-solvation energies vary depending on testing environments and solvation conditions, the values discussed here apply to aqueous solutions at 25°C. According to the Stokes' radius, ions with a smaller radius tend to have lower de-solvation energy.[71-73] As shown in Figure 1a,[74] K^+ and NH_4^+ (1.25 Å) have the smallest Stokes' radii, suggesting the lowest de-solvation energies in aqueous solutions. This reduced de-solvation energy is expected to lower energy consumption during the charge/discharge process.

To understand the kinetic advantages and disadvantages associated with NH_4^+, it is instructive to compare it with K^+ given their similarities in certain properties, such as hydrated and Stokes' radiuses. A key distinction between K^+ (and all other metal ions), which is spherical, and NH_4^+, which is tetrahedral, lies in their geometry. The asymmetric shape of NH_4^+ leads to a strong preferential orientation, influencing its electrochemical behavior in unique ways.

K^+ may form ionic bonds with electrode materials, partially disrupting its structure. The energy required to both form and break these bonds can affect the overall energy efficiency of the process and potentially compromise the stability of the electrode material's internal structure (as shown in Figure 1b). In contrast, during the insertion process into most host materials, NH_4^+ forms covalent hydrogen bonds (Figure 1c),[75] which have been shown to enhance the stability of the insertion process and providing structural integrity.[76]

Furthermore, at high concentrations, NH_4^+ can mitigate side reactions with the electrode and electrolyte, such as the oxygen evolution reaction (OER) and HER.[77] However, the formation and subsequent breaking of hydrogen bonds, while beneficial for stability, can be time-consuming. This may impact the rate of ion insertion and de-insertion at or near the surface of the electrode material, potentially limiting the performance of NH_4^+-based supercapacitors under high-rate currents. Additionally, the neutral nature of NH_4^+ in the electrolyte helps reduce electrode corrosion, thereby extending the service life of the device. This combination of factors makes NH_4^+ an intriguing option for supercapacitors while requiring further mechanistic understanding and electrode optimization to fully optimize

performance.

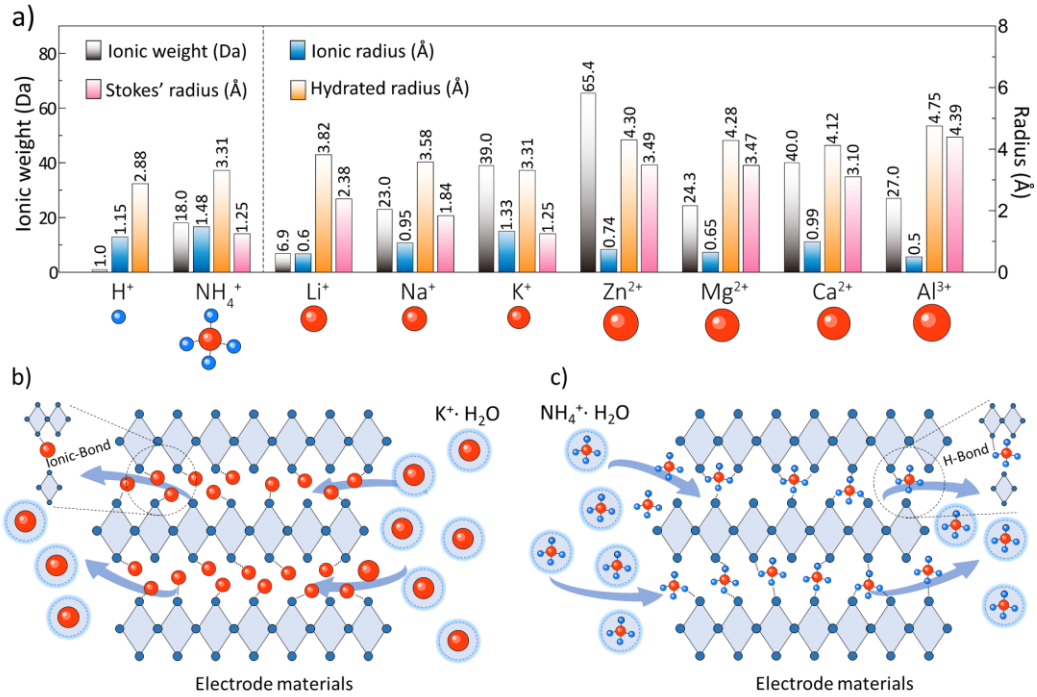

Figure 1. a) Comparison of the ionic weight, cation radius, Stokes' radius, and hydrated radius of the ammonium ion and conventional metal-ion charge carriers. b) Metal ions insertion into an electrode. c) NH_4^+ insertion into an electrode.

2.2 Aqueous electrolytes

The electrolyte is a critical component of supercapacitors, controlling not only the transport of charge carriers between the electrodes but also the kinetics of ion insertion/deinsertion. The classification of electrolytes tends to be less complex compared to that of charge carriers. Key to the behavior of electrolytes, whether they are metal or non-metal salt solutions, is their concentration. Concentrated electrolytes typically have concentrations exceeding ten or even tens of moles per liter. Here, we focus exclusively on the effects of dilute ammonium ion electrolytes on supercapacitors, since concentrated ammonium electrolytes have not yet been explored in supercapacitor applications.

The initial exploration of NH_4^+ in the field of energy storage can be traced back to research by Toshima et al. in 1982.[78] Subsequently, Cui et al. conducted pioneering work using Prussian blue analogues (PBAs) for NH_4^+ storage.[79] Ji et al. further advanced the concept by proposing the "rocking chair" ammonium ion battery, which validated the use of NH_4^+ as an effective charge/discharge carrier.[80] To date, much of the research involving ammonium ions has been focused primarily on batteries.

However, interest in utilizing NH_4^+ in supercapacitors has begun to grow in recent years. For example, Tang et al. developed a hybrid supercapacitor employing δ-MnO_2 as the cathode and activated carbon as the anode, using ammonium sulfate ($(NH_4)_2SO_4$) as the electrolyte.[81] This hybrid supercapacitor demonstrated a working voltage window of 2.0 V and achieved an energy density of 861.2 μWh cm^{-2}. Following this, other ammonium salts such as ammonium acetate (NH_4Ac), ammonium carbonate, and ammonium chloride (NH_4Cl) have also been employed as electrolytes in supercapacitors.[82-84] As noted above, the neutral to slightly acidic pH values of these NH_4^+-based electrolytes help prevent electrode corrosion, enhancing device longevity. Despite the cations in these electrolytes being identical, the performance of the supercapacitors is notably affected by the different anions present, which influence the capacity of the storage devices. Niu et al. highlighted this in their proposal for using highly concentrated $NH_4CF_3SO_3$ in ammonium batteries, which aimed to alter the solvation structure of NH_4^+ ions.[85] This adjustment is facilitated by $CF_3SO_3^-$ anions, which compete for the coordination position of water molecules, thereby illustrating the specific impact anions have on the solvation structure of ammonium ions. This nuanced understanding of ion interactions opens new avenues for optimizing electrolyte compositions in NH_4^+-based supercapacitors and other energy storage technologies.

One inherent limitation of diluted electrolytes is that the charging process leads to a reduction in the concentration of charge carrier ions within the electrolytes, due to their insertion into the electrode materials. This decrease in ion concentration directly impacts the conductivity of the electrolyte, subsequently influencing the rate performance of the electrode material. Furthermore, during the discharge process, the concentration of ammonium ions takes longer to recover compared to metal ions because breaking the hydrogen bonds formed during NH_4^+ insertion into the host electrode materials requires additional time. Therefore, high-concentration ammonium salt solutions may be more suitable as electrolytes for supercapacitors due to smaller fluctuations in concentration during the charge/discharge cycles. Moreover, higher concentrations can allow the working voltage windows of the supercapacitors to reach greater values. In a diluted electrolyte, ammonium ions are primarily coordinated with water molecules, and the maximum working voltage that these hydrated ammonium ions can withstand is constrained by the electrolysis potential of

water. Increasing the electrolyte concentration enhances the coordination interaction between the electrolyte anions and ammonium ions. This increased coordination limits the contact between water molecules and electrode materials, reducing side reactions and preventing the collapse of active materials. Therefore, the exploration of high-concentration ammonium ion electrolytes in supercapacitors represents a promising direction for future research, offering potential improvements in both performance and stability.

2.3 Mechanisms of ammonium ion insertion/desertion

Before exploring the mechanisms of ammonium ion insertion and desorption, it is essential to establish a basic understanding of electric double-layer (EDL) capacitance and pseudocapacitance. EDL capacitance arises from the electrostatic accumulation of charges at the interface between the electrode surface and the electrolyte. Pseudocapacitance, on the other hand, can be categorized into two main types: redox pseudocapacitance, which involves fast and reversible redox reactions occurring on or near the electrode surface, and intercalation pseudocapacitance, which entails the insertion of ions into the bulk of the electrode material without significantly altering its structure.

The b factor is commonly used to differentiate the contributions of diffusion-controlled and *surface capacitive* processes to the overall capacitance of a supercapacitor. It is derived from the relationship between the peak current (i) and the scan rate (v) in cyclic voltammetry: $i=av^b$. A b value of 0.5 indicates a purely diffusion-controlled process, while a b value of 1 signifies a surface-capacitive process, where *charge is stored through fast, reversible surface redox reactions, and electrostatic accumulation*. While significant variations in the b values of NH_4^+ have been reported, even when using the same type of electrode material, surface capacitive is often found to play a dominant role. For example, the b value of NH_4^+ in h-WO_3 host materials has been reported as 0.74, while in $(NH_4)_xWO_3$ it is 0.95.[84, 86] Various factors can influence b values, such as the host material's conductivity and electrolyte concentration. Additionally, NH_4^+ as a charge carrier exhibits different b values compared to other metal ions within the same host materials due to differences in bare ion radius and hydrogen bonding chemistry. For instance, in MoS_2 host materials, the b value for NH_4^+ is 0.81, while for Li^+ it is 0.90.[87] Therefore, further research is necessary to clarify and accurately predict the primary capacitance contributions in NH_4^+-based supercapacitors.

So far, ammonium ion-based supercapacitors have been assumed to primarily rely on the intercalation mechanism to achieve pseudocapacitance, regardless of whether the host materials have 1D, 2D, or 3D structures. This intercalation involves the insertion of ammonium ions into the host material's structure. Therefore, the current focus in designing ammonium ion supercapacitors is on developing host materials with suitable micro- and nanostructures that can effectively accommodate ammonium ions. These structural features enhance the ion intercalation process, improving overall device performance.

The distinct geometries, solvation/desolvation processes, and chemical bonding nature of metal and non-metal ions lead to different intercalation mechanisms. Typically, metal ions are accommodated between adjacent layers or within unoccupied tetrahedral or octahedral sites in host materials, where they form ionic bonds with lattice anions. Taking K^+ as an example, when K^+ ions are inserted into a metal oxide (MO_x, M=metal ion), they form K-O-M bonds. In contrast, NH_4^+ tends to form covalent bonds with host materials, which dynamically form and break as the ion intercalates into the host lattice. NH_4^+ acts as a Lewis acid (acceptor), bonding with electron-donating atoms in the electrode, which act as Lewis bases (donors). Consequently, materials that serve as Lewis bases and possess framework or layered structures are particularly well-suited for storing NH_4^+. These structures should maintain their integrity when NH_4^+ is inserted into interstitial positions. For example, PBAs, which have a face-centered cubic structure, remain stable during NH_4^+ intercalation.[80, 88, 89] Additionally, bi-layered V_2O_5 exhibits unique pseudocapacitive behavior with reversible NH_4^+ deintercalation and intercalation, highlighting its potential for energy storage applications.[90]

Owing to the relatively complex architecture of NH_4^+ compared to metal ions, the processes of NH_4^+ intercalation and diffusion are not straightforward and warrant further investigation. This complexity arises not only from the physical insertion but also from the intricate chemical interactions that occur during the charge and discharge cycles, making the study of NH_4^+ in energy storage systems a rich area for further research.

Additionally, materials characterized by defects and a higher number of active sites may facilitate a novel insertion mechanism: the co-insertion of NH_4^+ and H^+. This mechanism primarily hinges on two factors: material vacancies and low-concentration electrolytes. First, vacancies within the material structure enhance conductivity and electrochemical activity,

thereby promoting the chemistry of proton insertion. Second, the use of low-concentration electrolytes is crucial as it ensures that the co-insertion process proceeds smoothly.[91-93] Despite its potential, this insertion mechanism is still in the early stages of exploration, and further research is necessary to determine whether this mechanism competes with NH_4^+ for active sites or if it provides additional capacity.

2.4 Hydrogen bond formation/breaking

NH_4^+ features a tetrahedral geometry with a nitrogen atom at the center, surrounded symmetrically by four hydrogen atoms, forming a triangular pyramid. This unique shape endows NH_4^+ with a four-coordination solvation structure, which contributes to enhanced stability compared to the spherical geometry of metal ions. The hydrogen bonds formed between the oxygen atoms of water and the hydrogen atoms of ammonium differ fundamentally from the ionic bonds seen between metal ions and water molecules. In aqueous electrolytes, NH_4^+ is solvated as $NH_4^+(H_2O)_4$. Before NH_4^+ can intercalate into the lattice of host materials, it must undergo a desolvation process. This step requires energy to overcome the binding energy between NH_4^+ and the surrounding water molecules.

Once desolvated, NH_4^+ inserts into host materials in a manner akin to a monkey climbing a tree, using its four limbs to grasp and pull itself upward. During the process of NH_4^+ intercalation/deintercalation, hydrogen bonds are continuously formed and broken, which aids the ion in moving in and out of the host material's lattice. These covalent bonds enable electron delocalization by transferring electrons from the host materials to the ammonium ion, serving as an additional redox center. The exact nature of bond formation and the net ion intercalation depend on the specific characteristics of the electrode material. While the formation of hydrogen bonds generally boosts the electrode's stability, it also increases the time required for ion intercalation and deintercalation, which could affect the overall efficiency and rate performance of the energy storage system.

2.5 Diffusion mechanism

The diffusivity of charge carrier ions in electrolytes critically influences the capacity and rate performance of supercapacitors. Two primary diffusion scenarios can occur when electrolyte cations approach the electrode material. The first involves the adsorption of net charge carrier ions on and near the surface of electrode materials (Figure 2a). This scenario aligns with the

electric double layer (EDL) mechanism of supercapacitors, where the process occurs without Faradaic reactions. The second scenario involves intercalation-type or pseudocapacitive reactions, characterized by surface redox processes and intercalation at the surface or near-surface sites of the electrode materials (Figure 2b). This process falls under Faradaic reactions, which can deliver more energy for supercapacitors compared to adsorption diffusion. Currently, this intercalation-type mechanism is predominant in most ammonium-ion supercapacitors because the energy provided by simple adsorption diffusion is significantly limited.

For supercapacitors that rely primarily on adsorption diffusion, the electrode materials often require surface engineering to enhance their performance. An example of this is the work by Tang's group, which developed a phosphate ion-assisted surface functionalization strategy to increase the ammonium ion storage capacity of an α-MoO_3 electrode.[94] Their findings indicated that NH_4^+ intercalation into layered α-MoO_3 is not the primary mechanism; instead, charge storage relies significantly on the adsorption energy of surface oxygen atoms to NH_4^+. This insight highlights the importance of surface characteristics in optimizing the storage capacity and efficiency of NH_4^+-based supercapacitors. Table 1 lists several electrode materials used in NH_4^+-based supercapacitors and classified according to their channel type.

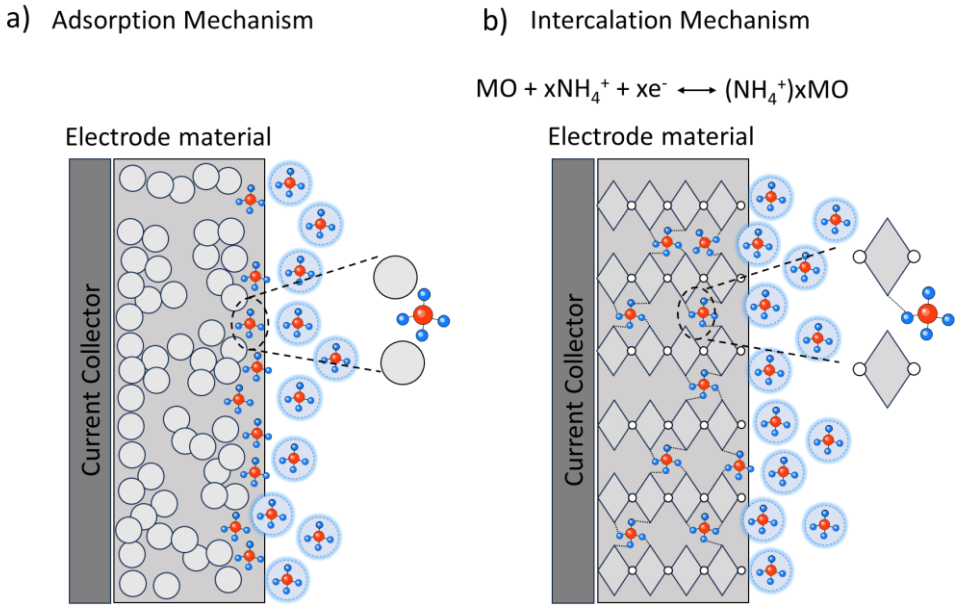

Figure 2. Schemes of the NH_4^+ adsorption (a) and intercalation (b) mechanisms.

Table 1. Channel types in electrode materials used in ammonium-ion supercapacitors.

Types	Channel type	Electrode materials
One dimensional	Tunnel channel	δ-MnO_2,[95] α-MnO_2,[96] MnO_2,[97]α-MoO_3,[116]
Two dimensional	Layered space	V_2O_5·nH_2O/rGo,[98] MoS_2@CC,[99] MoS_2@TiN/CNTF,[100] $(NH_4)_xWO_3$,[84] NVO,[101] $(NH_4)_2V_{10}O_{25}$·$8H_2O$,[102] KVO/PANI,[103] VOH/PEDOT,[104] ACC@VPP,[105] PVO,[106] SR-CoFe LDHs,[107] Od-NHVO,[108] MC_{700},[109] MoS_2@PANI,[87]
Three dimensional	Tunnel channel	$Fe_4[Fe(CN)_6]_3$,[110] $NaFe[Fe(CN)_6]$,[111]

3. Overview of Electrode Materials

The performance of supercapacitors, including their energy density and lifespan, strongly depends on the properties of electrode materials that determine ion/electron transfer and storage of charge carrier ions. Most inorganic materials such as PBAs, transition metal oxides, and layered compounds or sulfides are categorized as intercalation-type materials. These materials utilize their inherent tunnel channels or layered structures to accommodate NH_4^+ ions. For instance, 1D materials facilitate ion storage through tunnels, including quadrilateral and hexagonal tunnelling sites. 2D materials utilize appropriate interlayer spacings for ion storage, while 3D materials combine the storage capabilities of both 1D and 2D materials. The effectiveness of these structures is governed by their ability to accommodate the size of NH_4^+ ions within their channels or layers. In contrast, adsorption-type materials, which are predominantly organic, operate differently. Depending on the surface chemical composition of electrode material, NH_4^+ ions in the electrolyte can readily form hydrogen bonds with the oxygen (N-H···O), nitrogen (N-H···N), or sulfur (N-H···S) atoms in the electrode. Therefore, during the design phase, the surface or internal structure of organic compounds can be tailored through various functional groups to optimize these interactions. In this section, we delve into specific electrode materials that have been utilized in supercapacitors for ammonium ion storage, discussing their performance characteristics and the implications of their structural properties and composition on supercapacitor functionality. An overview of the electrode materials used as cathode and anode in ammonium ion supercapacitors is provided in Table 2.

Table 2. Electrode materials used in ammonium ion supercapacitors.

Electrode	Electrode Materials
Cathode	$Ti_2N/Ti_3C_2T_x$,[112] Cu-HHB/I_2,[113] KVO/PANI,[103] ACC@VPP,[105] VOH/PEDOT,[104] PVO,[106] $(NH_4)_2V_{10}O_{25}\cdot 8H_2O$,[102] δ-$MnO_2$,[95] MnO_2,[97] NVO,[101] α-MnO_2,[96] $V_2O_5\cdot nH_2O$,[98] MC_{700},[109] SR-CoFe LDHs,[107] Od-NHVO,[108] P-M-S,[114] MoS_2@CC,[99]
Anode	$(NH_4)_xWO_3$,[84] $(NH_4)_xV_2O_5$,[115] α-MoO_3,[116] MoS_2@TiN/CNTF,[100]

3.1 Metal oxides

Metal oxides, common in nature, are widely used as electrode materials in ammonium ion supercapacitors. For instance, Zhou's group developed a hybrid supercapacitor using a δ-MnO_2 cathode and an activated carbon anode (Figure 3a).[117] Leveraging the hydrogen bond chemistry of NH_4^+, this supercapacitor achieved a potential window of 2.0 V (Figure 3b).

Figure 3c illustrates the energy and power density of ammonium ion supercapacitors, showing that their energy density remains below 100 Wh kg^{-1}. Despite this current limitation, significant progress has been made in recent years with the development of advanced materials that exhibit optimized interlayer distances and enhanced electrical conductivity—both crucial factors for improving energy density in ammonium ion supercapacitor systems. This trend suggests that further refinement of these material properties could drive the energy density of ammonium ion supercapacitors to even higher levels.[39, 52, 96, 98, 103, 104, 106, 118-131]

In three-electrode system tests, the discharge time exceeded the charge time, indicating that NH_4^+ ions were trapped in δ-MnO_2, highlighting that the formation and breaking of hydrogen bonds are more time-consuming than those of ionic bonds (Figure 3d). The cycling performance of δ-MnO_2 electrode showed a 40% capacitance loss after 5000 cycles (Figure 3e). Additionally, ex-situ Raman measurements revealed that the intercalation/deintercalation of NH_4^+ could weaken the Mn-O bond in δ-MnO_2 (Figure 3f).[81]

Other studies have also explored MnO_2 for ammonium supercapacitors. Wang et al. investigated foam-like porous carbon nanosheets and oxygen-deficient α-MnO_2 as cathode and anode materials, respectively, in a hybrid supercapacitor.[96] The devices delivered a specific capacitance of 180.8 F g^{-1} at 0.5 A g^{-1} and achieved 64.2 Wh kg^{-1} at a power density of 400 W kg^{-1} within a 1.6 V potential window in a two-electrode system. FT-IR analysis indicated that

the intensity of N-H-O and N-H bonds fluctuated with charging and discharging, evidencing the dynamic formation and breaking of hydrogen bonds; unchanging peaks post-discharge indicated residual NH_4^+ adsorption at oxygen vacancy sites. Dubal's group reported that the phase of MnO_x transformed from amorphous to birnessite type during charging/discharging, with time-of-flight secondary ion mass spectrometry confirming effective NH_4^+ intercalation into layered MnO_x.[97] Their MnO_x electrodes achieved a specific capacitance of 175.0 F g^{-1} at 1.0 A g^{-1} and maintained 89% capacitance retention after 1000 cycles in a three-electrode system. Their assembled aqueous ammonium ion capacitor exhibited an energy density of 15.93 Wh kg^{-1} with 90% cycling stability after 5000 cycles.

In addition to Mn-based oxides, vanadium-based oxides are also widely used in ammonium ion supercapacitors due to their rich valence states and layered structures. Zhang et al. used ammonium vanadium oxide electrodes with an NH_4Cl/PVA gel electrolyte in a three-electrode system, delivering a specific capacitance of 339.0 F g^{-1} at 0.5 A g^{-1}, with 71% capacitance retention after 14,000 cycles.[127] Their flexible quasi-solid-state device maintained over 67% capacitance retention after 12,000 cycles, delivering 324 mF cm^{-2} at 1 mA cm^{-2}. Zhang's group also developed a free-standing vanadium oxide hydration/reduced graphene oxide (VGF) film for flexible ammonium ion supercapacitors.[98] The flexible composite film, like paper, makes wearable applications of ammonium ion supercapacitors possible. The VGF electrode exhibited a specific capacitance of 600 F g^{-1} at 0.2 A g^{-1}, and the assembled symmetric supercapacitor displayed 0.82 Wh m^{-2} at 0.09 W m^{-2}, with an outstanding capacitance retention of 92.0 % after 20,000 cycles.

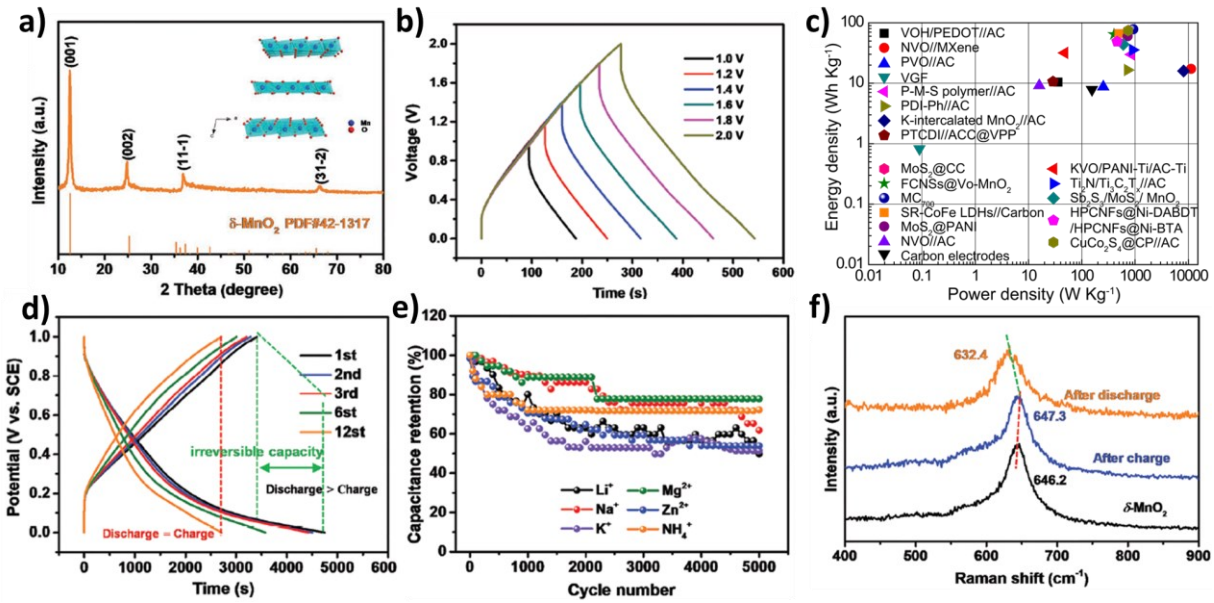

Figure 3. a) XRD pattern of δ-MnO_2. b) GCD curves of the MnO_2//ACC A-HSCs collected at different voltage windows at a fixed current density of 8 mA cm^{-2}. c) Ragone plot including various ammonium ion supercapacitors. d) Selected GCD profiles from the initial 12 cycles at 2 mA cm^{-2}. e) Cycling performance. f) Ex situ Raman. Reproduced from Ref. [117] with permission from Wiley.

MoO_3 has also been explored as a promising material for ammonium ion supercapacitors. We developed a thermal treatment strategy to prepare electrodes from MoO_3@C composites.[26] Within ammonium ion supercapacitors, the as-prepared MoO_3@C composites exhibited impressive electrochemical performance, delivering a specific capacitance of 473.0 F g^{-1} at 1.0 A g^{-1} and maintaining 92.7% of capacitance retention after 5,000 cycles. Density functional theory (DFT) calculations provided insights into the mechanism behind the composite's performance, demonstrating that oxygen vacancies enhance both ionic and electronic transport within the composite. These vacancies also boost the electrochemical reaction sites, while simultaneously facilitating the formation of hydrogen bonds between NH_4^+ ions and the host material (Figures 4a-c). The symmetric supercapacitors made from these composites achieved energy densities above 78 Wh kg^{-1} at a power density of 929 W kg^{-1}, with an impressive capacitance retention of 97.6% after 10,000 cycles under a potential window of 1.8 V (Figures 4d,e). This study underscores the advantageous role of non-metal charge carriers like NH_4^+ and highlights the positive impact of oxygen vacancies on the storage capabilities of ammonium ions.

Despite these advancements, challenges remain with metal oxides, such as propensity for agglomeration, structural instability, and specially limited conductivity, which can hinder the performance of aqueous supercapacitors.

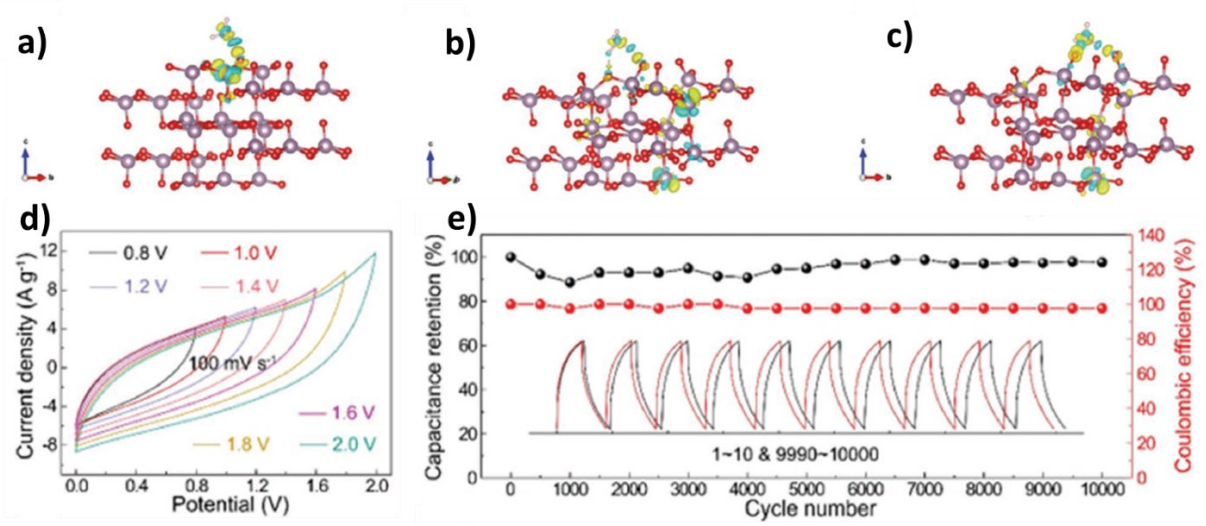

Figure 4. a) Differential charge density of NH_4^+ adsorbed on pristine MoO_3 (020), b) at the Mo site, and c) at the O vacancy site on the oxygen-deficient MoO_3. d) CV curves at various potential windows. e) Cycling performance and Coulombic efficiency at 10 A g^{-1}. Reproduced from Ref. [26] with permission from Wiley.

3.2 Metal sulfides

Compared to metal oxides, sulfides generally exhibit higher intrinsic electronic conductivity, which can significantly benefit device performance. Sulfides are frequently semiconductors with relatively small band gaps which can be further reduced upon NH_4^+ intercalation. As an example, Han's group has used 2H-MoS_2 for ammonium ion supercapacitors, where DFT calculations confirmed that NH_4^+ intercalation/deintercalation is governed by a pseudocapacitive charge storage process involving the bonding and breaking of H-S bonds.[82] Interestingly, the semiconductor nature of 2H-MoS_2 transitions to metallic after NH_4^+ intercalation, illustrating how the phase structure of materials can be altered by intercalating ions (Figures 5a-d). The 2H-MoS_2 electrode achieves a high capacitance of 1,010 F g^{-1} at 1 A g^{-1} and maintains 92% of its specific capacitance after 10,000 cycles. When configured in a symmetric device under a 1.5 V potential window, it reaches an energy density of 74.23 Wh kg^{-1} at a power density of 751 W kg^{-1}.

Additionally, there is growing interest in flexible ammonium-ion asymmetric

supercapacitors. Li et al. developed a core-shell structure of MoS_2@TiN/CNTF specifically for flexible supercapacitors.[83] This heterostructure electrode delivers a specific capacitance of 1102.5 mF cm^{-2} at 2 mA cm^{-2}, and the quasi-solid-state fiber-shaped asymmetric supercapacitors achieve an energy density of 195.1 μWh cm^{-2} under a 2.0 V potential window. DFT calculations in their study confirmed a significant enhancement in the binding strength of ammonium ions to the MoS_2 shell layer within the heterostructure, where a built-in electric field accelerates charge transfer.

We combined MoS_2 with polyaniline to create composite electrodes for ammonium ion supercapacitors.[132] Our findings indicate that vacancies in MoS_2@PANI enhance both the conductivity and adsorption capabilities of the electrode. Capacitance contribution analysis suggests that the unique insertion mechanism of NH_4^+ could significantly improve electrochemical performance, particularly in terms of stability, compared to metal cations (Figures 5e-g). While the formation of hydrogen bonds with the host material may slow the rate performance, the relatively low mass of NH_4^+ facilitates its intercalation and fast diffusion within the electrolyte. The composites exhibit a specific capacitance of 452 F g^{-1} at 1 A g^{-1}, with 86.3% capacitance retention after 5,000 cycles in a three-electrode setup.[132]

3.3 Other 2D inorganic materials

To date, the use of oxides or sulfides in ammonium ion supercapacitors remains limited. A key challenge is the inappropriateness of the micro-nano structure of materials, which often does not suit the specific needs of supercapacitor applications. Similar to MoS_2 and MoO_3, materials with layered structures like MXene and layered double hydroxides have also garnered attention recently. Han et al. synthesized N-functionalized 2D MXene ($Ti_3C_2T_x$) with Ti_2N interface engineering ($Ti_2N/Ti_3C_2T_x$).[129] Their experimental studies and DFT calculations demonstrated that interface engineering enhances rapid electron transport, provides higher specific capacitance, and improves rate capability. Ex-situ XRD analysis showed that the characteristic peak of Ti_2N remained stable during the charge/discharge process, indicating a highly reversible NH_4^+ intercalation/deintercalation process. Ex-situ XPS tests revealed that the O-H bond peak decreases during the discharge process and increases upon recharging, highlighting the coupling of NH_4^+ with solvent H_2O molecules.

Wang's group developed structurally reconstructed cobalt-iron layered double hydroxides

(SR-CoFe LDHs) for ammonium supercapacitors.[124] The capacitance of the as-prepared SR-CoFe LDHs electrode was found to be 3.3 times higher than that of the pristine material. Theoretical calculations suggest that the presence of structural defects in the CoFe-LDHs reduces the NH_4^+ adsorption energy and induces electron delocalization, thereby enhancing electrical conductivity (Figure 5h,i). The hybrid supercapacitor developed using these materials delivers a substantial specific capacitance of 238.3 F g^{-1}, and a high energy density of 66.2 Wh kg^{-1} within a wide working voltage of 2.0 V.

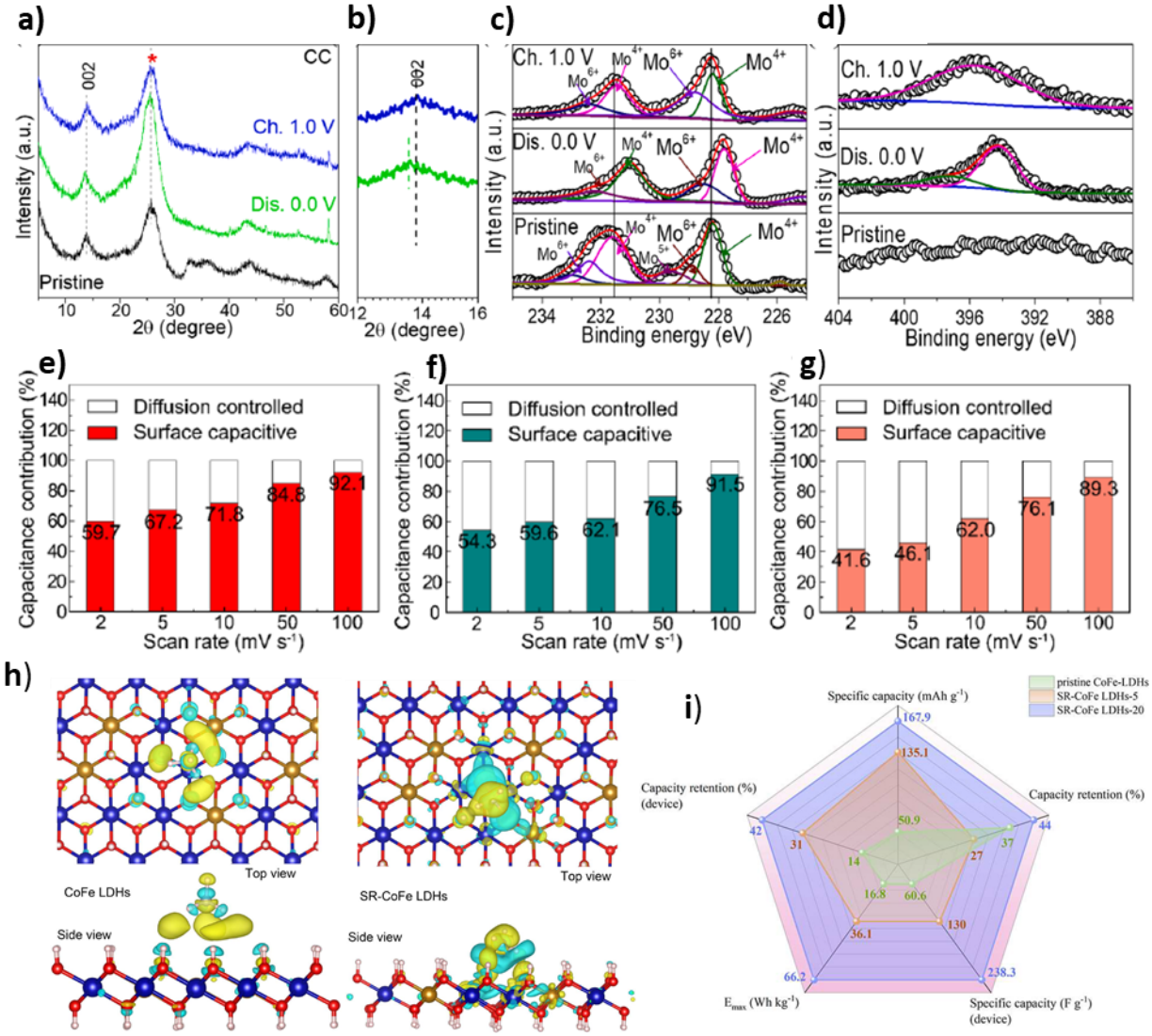

Figure 5. Post-mortem analysis of a MoS_2@CC cathode to determine the NH_4^+ storage mechanism: a-b) XRD patterns, c) XPS of Mo-3d, d) N-1s. Reproduced from Ref. [82] with permission from Elsevier. e) Ratio of the surface capacitive contribution to total capacity at various scan rates for Li^+, f) K^+ and g) NH_4^+. Reproduced from Ref. [132] with permission from Wiley. h) Charge density difference distribution diagrams for NH_4^+ in pristine CoFe LDHs and SR-CoFe LDHs. The yellow region shows charge accumulation and the cyan region means charge depletion. i) The radar diagram for pristine CoFe-LDHs//HC, SR-CoFe LDHs-5//HC and

SR-CoFe LDHs-20//HC. Reproduced from Ref. [124] with permission from Wiley.

3.4 Pre-intercalated materials

Over time, any type of electrode immersed in an aqueous electrolyte will eventually experience structural collapse. Tang's group demonstrated that pre-intercalating NH_4^+ into electrodes can stabilize the tunnel structure and significantly enhance both the service life and capacitance of the devices.[84] They utilized a pre-intercalation strategy to assemble an asymmetric supercapacitor based on an $(NH_4)_xWO_3$ anode paired with an α-MnO_2 cathode. This configuration delivered an impressive area capacitance of 2,239.7 mF cm^{-2} and a peak areal energy density of 1,010.1 mWh cm^{-2}. DFT calculations indicated that the pre-intercalated tunnel-structured h-WO_3 effectively enhances the NH_4^+ adsorption energy and reduces the NH_4^+ diffusion energy barrier (Figure 6a). Ex situ XRD and XPS analyses confirmed that the intercalation and deintercalation of NH_4^+ are accompanied by the formation and breaking of hydrogen bonds, providing a deeper understanding of the storage mechanism of NH_4^+ in tunnel-structured inorganic materials.

In a similar vein, Zhan et al. developed a $(NH_4)_2V_{10}O_{25}\cdot 8H_2O$ structure that harnesses a two-electron redox process, significantly enhancing the electrochemical performance of aqueous supercapacitors.[133] By incorporating trace amounts of NH_4I into the $(NH_4)_2SO_4$ electrolyte, the specific capacitance of the supercapacitor increased from 200.8 F g^{-1} to 562.5 F g^{-1}, a benefit attributed to additional chemical reactions (Figure 6b). The asymmetric device demonstrated an energy density of 50.5 Wh kg^{-1} and maintained 74.9% capacity retention after 5,000 cycles, showcasing the beneficial synergistic effect of the electrodes and electrolytes. This work provides valuable insights for future research into electrode–electrolyte synergy, highlighting innovative ways to improve supercapacitor performance and durability.

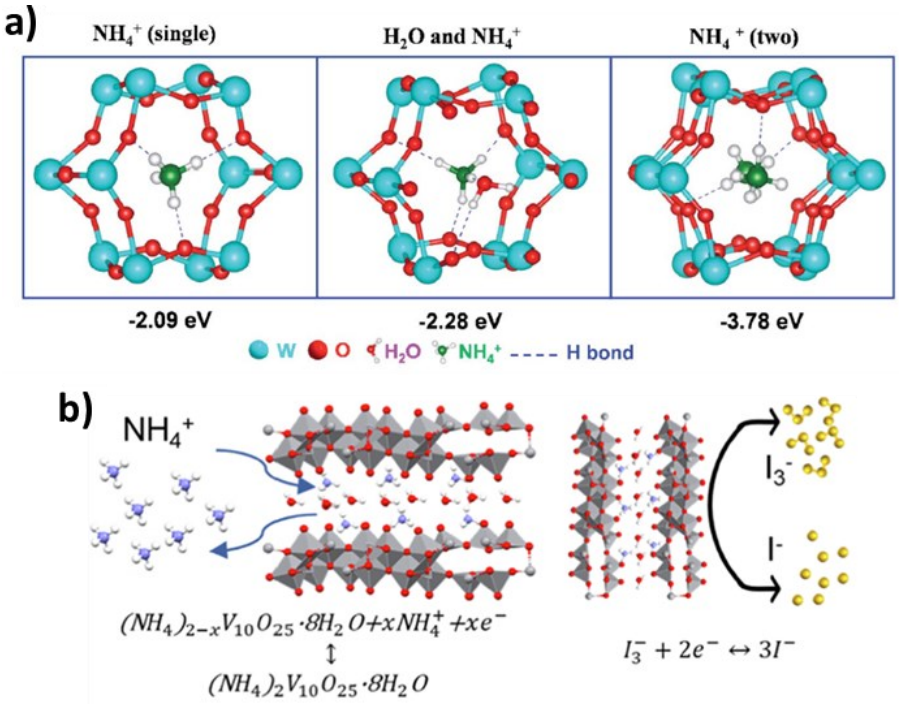

Figure 6. a) Schematic diagram of the three bonding states and adsorption energy in the WO_3 tunnel structure: single NH_4^+, H_2O and NH_4^+, and two NH_4^+ intercalations. Reproduced from Ref. [84] with permission from Royal society of chemistry. b) Schematic diagram of NVO energy storage process. Reproduced from Ref. [133] with permission from Elsevier.

3.5 Organic-inorganic and fully organic materials

Organic/inorganic composite materials are also commonly used in ammonium supercapacitor electrodes. Recent studies have shown the effectiveness of polymer intercalation strategies in expanding the inorganic lattice, thereby enhancing ion intercalation within these composite electrodes. This method not only boosts the electrochemical performance of the electrodes but also strengthens their structural stability and improves ion transport properties, leading to more efficient and durable supercapacitors.

As an example, Zhang et al. implemented a polymer intercalation strategy to expand the interlayer spacing of inorganic hosts, enhancing kinetics and stabilizing the structure during NH_4^+ deintercalation.[134] Specifically, polyaniline was intercalated into the interlayer space of hydrated vanadium oxide, increasing the interlamellar spacing from 11.0 Å to 13.9 Å (Figures 7a,b). This expansion allowed the specific capacitance of the vanadium oxide sample to rise from 156 F g^{-1} to 351 F g^{-1} at a current of 1 A g^{-1}. However, the material exhibited poor cycle stability, with a capacitance retention of only 56% after 10,000 cycles. To address this issue, Zhang et al. employed polyvinyl alcohol to develop a quasi-solid-state PVA/NH_4Cl electrolyte.

The PVA gel electrolyte acts to inhibit electrochemical dissolution and prevent the collapse of the PANI-intercalation-hydrated vanadium oxide (PVO) crystal structure, enhancing the durability of the supercapacitor.

Furthermore, Zhang et al. explored additional polymers for interlayer expansion, including poly(3,4-ethylenedioxythiophene) (PEDOT), K+/polyaniline, and poly(3,4-ethylenedioxythiophene)-poly(styrenesulfonate) (PEDOT:PSS).[104, 135, 136] For instance: 1) poly(3,4-ethylenedioxythiophene) intercalated into hydrated vanadium oxide (HVO) delivers a specific capacitance of 327 F g^{-1} at 1 A g^{-1} (Figure 7c,d). A quasi-solid-state HVO/PEDOT//active carbon hybrid supercapacitor constructed with this material demonstrated a capacitance of 328 mF cm^{-2} at 1 mA cm^{-2}. 2) K^+/polyaniline was intercalated into hydrated vanadium oxide, benefiting from the synergistic effect of co-intercalation which optimized the intercalation pseudocapacitive behavior. The electrode delivered a specific capacitance of 340 F g^{-1} at 0.5 A g^{-1}. 3) Poly(3,4-ethylenedioxythiophene)-poly(styrenesulfonate) was intercalated into vanadium oxide hydrate (VOH), expanding the V-O interlayer space and facilitating rapid ion diffusion. The resulting materials provided a capacitance of 511 F g^{-1} at 0.5 A g^{-1}.

Beyond organic/inorganic composites, organic-inorganic materials such as metal-organic frameworks (MOFs) and particularly 2D MOFs have been also recently explored for ammonium ion supercapacitors. Feng et al. developed a Cu-HHB (hexahydroxybenzene) MOF embedded with iodine (Cu-HHB/I_2), which offers rich accessible active sites of copper-bis(dihydroxy) (Cu-O_4) and iodide species.[51] This configuration achieved an areal capacitance of 111.7 mF cm^{-2} at 0.4 mA cm^{-2}. Theoretical calculations suggested that Cu-O_4 species could bind polyiodide, preventing its dissolution and contributing to the pseudocapacitance. When combined with MXene, the hybrid supercapacitors produced by this MOF delivered an energy density of 31.5 mWh cm^{-2}, with an impressive 89.5% capacitance retention after 10,000 cycles.

All-organic ammonium ion supercapacitor electrode materials are also gaining attention. For instance, Balaraman et al. synthesized organic polymer electrode materials by linking perylenetetracarboxylic diimide units through monosulfide and disulfide groups.[119] The optimal sample delivered a specific capacitance of 196 F g^{-1} at a current density of 1 A g^{-1} using 27 M ammonium acetate, showcasing the potential of organic materials in ammonium ion supercapacitor applications.

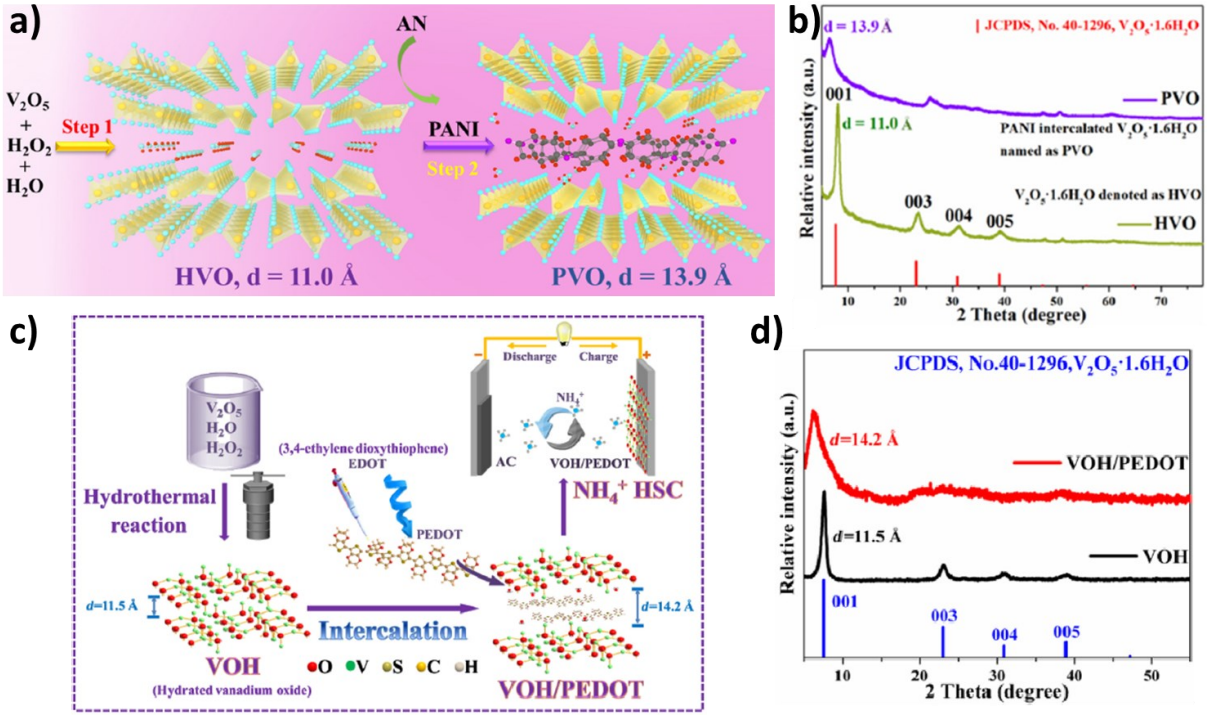

Figure 7. a) Illustration of the synthesis process of PVO and the variable lattice spacing. b) Characterizations of PVO and HVO: XRD patterns. Reproduced from Ref. [134] with permission from Elsevier. c) Flow diagram of synthesizing VOH/PEDOT material. d) Characterizations of VOH and VOH/PEDOT: XRD patterns. Reproduced from Ref. [121] with permission from Elsevier.

3.6 Other

In addition to the electrode materials above mentioned, other innovative material design and engineering approaches, including surface and defect engineering, have been applied to obtain high-performance ammonium ion supercapacitor electrodes. As an example, Tang's group employed a surface functionalization strategy, using phosphate decorations on α-MoO_3.[116] Theoretical calculations and electrochemical analysis revealed that in the ammonium ion supercapacitor system, NH_4^+ intercalation into layered α-MoO_3 is not the primary mechanism; instead, charge storage largely depends on the adsorption energy of surface oxygen atoms to NH_4^+ (Figure 8a). This surface engineering significantly enhanced the structural stability of the composites, with the optimized samples maintaining 69.5% capacitance retention after 2,500 cycles.

Defect engineering has proven to be an effective method for developing high-performance electrode materials. Zhang et al. created an oxygen-defective ammonium vanadate with a 3D

porous flower-like architecture for use in flexible quasi-solid-state ammonium ion hybrid supercapacitors (Figure 8b).[137] The introduction of oxygen vacancies not only improved electrical conductivity but also provided additional active sites and unblocked channels, facilitating fast reaction kinetics and ensuring stable capacitance. The optimized samples demonstrated a specific capacitance of 505 F g^{-1} at 0.5 A g^{-1} and maintained 80% capacitance retention after 10,000 cycles (Figure 8c,d).

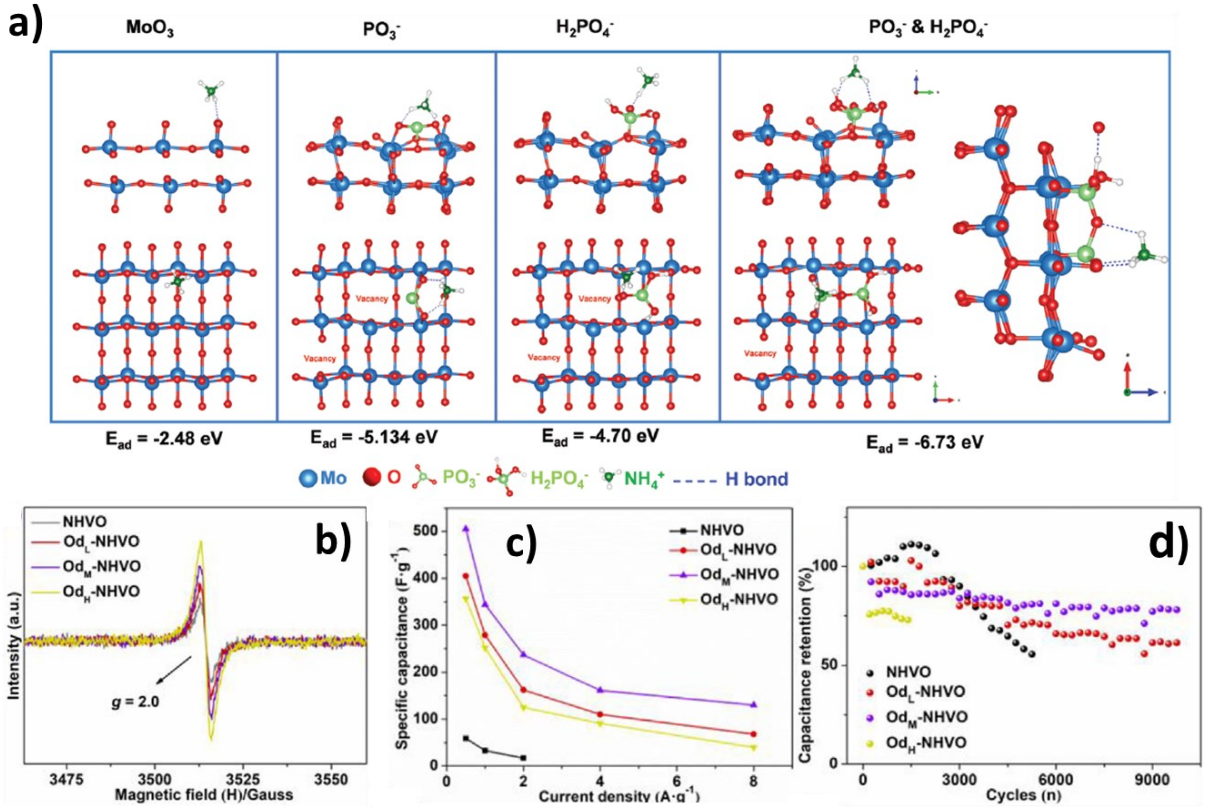

Figure 8. a) Schematic diagram of four bond states and adsorption energy of single NH_4^+ adsorbed on the surface of MO_3 structure: MoO_3, MoO_3 adsorbed with PO_3^-, $H_2PO_4^-$, and PO_3^- &$H_2PO_4^-$. Reproduced from Ref. [116] with permission from Wiley. Characterizations of NHVO and various Od-NHVO, b) EPR spectra, c) specific capacitance, d) cycling stability. Reproduced from Ref. [137] with permission from Elsevier.

4. Summary and Perspectives

This review highlights the advantages of using non-metallic ions, specifically ammonium ions, as charge carriers. These advantages include their high ionic conductivity, which supports enhanced capacity performance. The abundance of ammonium ions and their compatibility with aqueous solutions ensure low cost and high safety, making them ideal for large-scale stationary applications, portable electronics, and vehicles. Ammonium ions also benefit from

fast transfer kinetics and low desolvation energy due to their small hydrated ionic radius and Stokes' radius. The flexibility of hydrogen bonds between NH_4^+ and electrode materials during the insertion process enhances the electrochemical properties and stabilizes the electrode materials. To provide a clearer image of the state of the art in ammonium ion supercapacitors, key data is compiled in Table 3. This table includes data for various electrolytes such as $(NH_4)_2SO_4$, NH_4Cl, NH_4Ac, and PVA/NH_4Cl. Most ammonium ion supercapacitors operate under wide potential windows (exceeding 1 V), and their cycle stability competes favorably with that of lithium-ion batteries. However, the energy density of these supercapacitors remains a challenge, with specific capacitances typically ranging from 300 to 600 F g^{-1}. This indicates room for significant improvement in the performance of ammonium ion supercapacitors.

In terms of electrode materials, those that offer adequate space for storing ammonium ions and can form hydrogen bonds with them are preferred. Besides, they should prevent HER /OER during the NH_4^+ insertion/extraction process. Currently, just a few materials, mainly metal oxides or layered inorganic materials, have been optimized as electrode materials in ammonium ion supercapacitors, yet many other materials could potentially be suitable. PBAs serve as a pertinent example. They are frequently used in ammonium ion batteries with organic electrolytes but less so in supercapacitors, particularly those with aqueous electrolytes. The structural characteristics of PBAs make them suitable to provide high electrochemical performance across wide potential windows. PBAs typically have a suitable working window that exceeds 1.23 V, which is higher than the electrolysis voltage of water. To take full advantage of PBAs as electrode materials, high-concentration electrolytes can be tried in PBAs-ammonium supercapacitors, or building organic-inorganic hybrid materials.

The exploration of organics in this field is still in the early stages. The development and utilization of organic-inorganic hybrid materials or purely organic materials could become focal points for future research. Organic-inorganic hybrid materials are particularly promising because organic components can be functionalized to adsorb NH_4^+, while inorganic materials provide structural channels or layers for storing NH_4^+. These materials should be easy to prepare, cost-effective, safe, and recyclable.

Additionally, continued investigation into new electrolytes such as concentrated electrolytes, hydrogel electrolytes, and those containing additives is crucial to enhance the conductivity,

safety, and overall performance of supercapacitors. For electrolytes, those that maintain stable physical and chemical properties under wide working potential windows without parasitic side reactions are ideal. They should also have a suitable pH value that is weakly acidic to neutral to be gentle on electrode materials. Salt-in-water ammonium ion electrolytes are notable for their high ionic conductivity, and anion-doped electrolytes should also be considered.

Further in-depth investigation is necessary to explore whether hydrogen bonds can provide more energy than ionic bonds and to elucidate how ammonium ions intercalate into various electrode materials. The possibility of co-intercalation of ammonium and hydrogen ions into electrode materials, and whether there is a sequence to their insertion, warrants further study. Additionally, the development of ammonium ion flexible supercapacitors should be pursued.

As an emerging field, aqueous ammonium ion supercapacitors present significant potential for real-world energy storage applications, deserving broader consideration and continued research investment.

Table 3. Comparison of representative electrode materials for ammonium ion supercapacitors

Electrode materials	Electrolyte	Working window	Capacity	Capacity retention	Energy density	Ref.
δ-MnO_2	$(NH_4)_2SO_4$	0.0~1.0	9.5 F·cm^{-2} at 2 mA·cm^{-2}	60%/5000	861.2μWh·cm^2	81
V_2O_5·nH2O/rGo	PVA/NH_4Cl	-0.2~1.0	600.0 F·g^{-1} at 0.2 A·g^{-1}	93%/10,000	0.82 Wh·m^{-2}	138
α-MnO_2	$(NH_4)_2SO_4$	-0.7~0.3	525.1 F·g^{-1} at 0.5 A·g^{-1}	94.1%/10,000	64.2 Wh·kg^{-1}	96
MnO_2	$(NH_4)_2SO_4$	0.0~1.0	175.0 F·g^{-1} at 1.0 A·g^{-1}	~89.0%/1000	15.9 Wh·kg^{-1}	97
MoS_2@CC	$(NH_4)_2SO_4$	0.0~1.0	1010.0 F·g^{-1} at 1.0 A·g-^{1}	98.0%/10,000	74.2 Wh·kg^{-1}	82
MoS_2@TiN/CNTF	NH_4Cl	-0.8~0.0	1.1 F·cm^{-2} at 2 mA·cm^{-2}	82.0%/1000	351.2μWh·cm^2	83
$(NH_4)_xWO_3$	NH_4Ac	-0.8~0.2	8.0 F·cm^{-2} at 2 mA·cm^{-2}	85.8%/5000	1010.1μWh·m^{-2}	84
NVO	PVA/NH_4Cl	-0.8~1.0	339.0 F·g^{-1} at 0.5 A·g^{-1}	71.0%/14,000	9.1 Wh·kg^{-1}	101
$(NH_4)_2V_{10}O_{25}$·$8H_2O$	$(NH_4)_2SO_4/I^-$	-0.4~0.8	562.5 F·g^{-1} at 1.0 A·g^{-1}	74.9%/5000	40.2 Wh·kg^{-1}	133

KVO/PANI	PVA/NH_4Cl	-0.2~0.9	340.0 $F \cdot g^{-1}$ at 0.5 $A \cdot g^{-1}$	63.0%/10,000	31.8 $Wh \cdot kg^{-1}$	136
VOH/PEDOT	PVA/NH_4Cl	-0.2~1.0	327.0 $F \cdot g^{-1}$ at 0.5 $A \cdot g^{-1}$	52.0%/10,000	10.4 $Wh \cdot kg^{-1}$	104
ACC@VPP	PVA/NH_4Cl	-0.5~1.0	511.0 $F \cdot g^{-1}$ at 0.5 $A \cdot g^{-1}$	72.0%/10,000	3.2 $Wh \cdot m^{-2}$	135
PVO	PVA/NH_4Cl	-0.2~1.0	351.0 $F \cdot g^{-1}$ at 1.0 $A \cdot g^{-1}$	56.0%/10,000	17.5 $Wh \cdot kg^{-1}$	134
α-MoO_3	NH_4Ac	-1.0~-0.1	15.3 $F \cdot cm^{-2}$ at 2 $mA \cdot cm^{-2}$	69.5%/2500	2.4 $Wh \cdot cm^{-2}$	116
SR-CoFe LDHs	$(NH_4)_2SO_4$	0.0~1.0	167.9 $mAh \cdot g^{-1}$ at 0.5 $A \cdot g^{-1}$	91.0%/10,000	66.2 $Wh \cdot kg^{-1}$	139
Od-NHVO	PVA/NH_4Cl	-0.8~1.0	505.0 $F \cdot g^{-1}$ at 0.5 $A \cdot g^{-1}$	~80.0%/10,000	3.0 $Wh \cdot m^{-2}$	137
P-D-S	NH_4Ac	-1.0~0.1	167.0 $F \cdot g^{-1}$ at 1.0 $A \cdot g^{-1}$	72.0%/10,000	29.9 $Wh \cdot kg^{-1}$	140
MC_{700}	$(NH_4)_2SO_4$	-0.6~0.6	473.0 $F \cdot g^{-1}$ at 1.0 $A \cdot g^{-1}$	92.7%/5000	78.0 $Wh \cdot kg^{-1}$	26
MoS_2@PANI	NH_4Cl	-0.6~0.4	450.0 $F \cdot g^{-1}$ at 1.0 $A \cdot g^{-1}$	86.3%/5000	60.0 $Wh \cdot kg^{-1}$	132

Declaration of Competing Interest

The authors declare that they have no known competing financial interests or personal relationships that could have influenced the work reported in this paper.

Acknowledgments

The authors acknowledge funding from Generalitat de Catalunya 2021SGR01581 and European Union Next Generation EU/PRTR. D.J. thanks the scholarship support by the China Scholarship Council (202206310046-DAI JUGUO).

Reference.

1. J. Dai, Y. Lv, J. Zhang, D. Zhang, H. Xie, C. Guo, A. Zhu, Y. Xu, M. Fan, C. Yuan and L. Dai, *J Colloid Interface Sci*, 2021, **590**, 591-600.
2. J. Dai, S. Zeng, Y. Lv, H. Xie, L. Luo, Y. Xu and L. Dai, *Electrochim Acta*, 2021, **378,** 138149.
3. J. Dai, L. Luo, X. Wang, L. Xia, H. Xie, C. Yang, R. Wang, Y. Xu and L. Dai, *Mater Chem Phys*, 2022, **287**, 126224.
4. C. Huang, J. Yu, C. Y. Zhang, Z. B. Cui, J. K. Chen, W. H. Lai, Y. J. Lei, B. F. Nan, X. Lu, R. He, L. Gong, J. S. Li, C. H. Li, X. D. Qi, Q. Xue, J. Y. Zhou, X. Q. Qi, L. Balcells, J. Arbiol and A. Cabot, *Adv Mater*, 2400810.
5. J. S. Li, L. M. Li, J. Wang, A. Cabot and Y. F. Zhu, *Acs Energy Lett*, 2024, **9**, 853-879.
6. L. Gong, C. Y. Zhang, J. S. Li, G. Montaña-Mora, M. Botifoll, T. Z. Guo, J. Arbiol, J. Y. Zhou, T. Kallio, P. R.

Martínez-Alanis and A. Cabot, *Acs Appl Mater Inter*, 2024, **16**, 6948-6957.
7. G. F. Zeng, Q. Sun, S. Horta, S. Wang, X. Lu, C. Y. Zhang, J. Li, J. S. Li, L. J. Ci, Y. H. Tian, M. Ibáñez and A. Cabot, *Adv Mater*, 2024, **36**, 2305128.
8. C. Y. Zhang, X. Lu, X. Han, J. Yu, C. Q. Zhang, C. Huang, L. Balcells, A. G. Manjón, J. J. Biendicho, J. S. Li, J. Arbiol, G. Z. Sun, J. Y. Zhou and A. Cabot, *J Am Chem Soc*, 2023, 145, 18992-19004
9. C. Huang, J. Yu, C. H. Li, Z. B. Cui, C. Q. Zhang, C. Y. Zhang, B. F. Nan, J. S. Li, J. Arbiol and A. Cabot, *Adv Funct Mater*, 2023, **33**, 2305624.
10. J. Liu, Y. H. Zhou, T. Y. Yan and X. P. Gao, *Adv Funct Mater*, 2024, **34**, 2309625.
11. Q. Zhang, S. Jiang, T. T. Lv, Y. Peng and H. Pang, *Adv Mater*, 2023, **35**, 2305532.
12. K. Luo, M. Zhou, T. Liu, X. Q. Zhuge, T. X. Liu, M. Bayati, Y. R. Ren and Z. H. Luo, *Small Struct*, 2023, **4**, 2300107.
13. Y. Li, J. H. Li, Y. Ding, X. N. Feng, X. Liu, P. F. Yan, M. L. Sui and M. G. Ouyang, *Energy Storage Mater*, 2024, **65**, 103167.
14. M. M. Wang, Y. H. Meng, Y. Xu, N. Chen, M. Y. Chuai, Y. Yuan, J. F. Sun, Z. C. Liu, X. H. Zheng, Z. Q. Zhang, D. J. Li and W. Chen, *Energ Environ Sci*, 2023, **16**, 5284-5293.
15. Z. X. Shi, Z. N. Tian, D. Guo, Y. Z. Wang, Z. Bayhan, A. S. Alzahrani and H. N. Alshareef, *Acs Energy Lett*, 2023, **8**, 3054-3080.
16. C. Zhu, C. Sun, R. Li, S. Weng, L. Fan, X. Wang, L. Chen, M. Noked and X. Fan, *ACS Energy Letters*, 2022, **7**, 1338-1347.
17. L. Xu, J. Li, Y. Xiang, Y. Tian, R. Momen, H. Liu, F. Zhu, H. Tu, Z. Luo, S. Fang, W. Deng, G. Zou, H. Hou and X. Ji, *Energy Storage Materials*, 2022, **52**, 655-663.
18. S. Abdul Ahad, S. Bhattacharya, S. Kilian, M. Ottaviani, K. M. Ryan, T. Kennedy, D. Thompson and H. Geaney, *Small*, 2023, **19**, 2205142.
19. C. Y. Xiaoli Su, Xinpeng Li, Minghao Guo, Ruiguo Cao, Kun Ni *, Yanwu Zhu *, *Energy Storage Materials*, 2022, **50**, 365-372.
20. Y. Katsuyama, N. Haba, H. Kobayashi, K. Iwase, A. Kudo, I. Honma and R. B. Kaner, *Adv Funct Mater*, 2022, **32**, 2201544.
21. M. Usselmann, J. Bansmann and A. J. C. Kuehne, *Adv Mater*, 2023, **35**, 2208484.
22. Q. Wang, Y. X. Qu, J. Bai, Z. Y. Chen, Q. T. Luo, H. J. Li, J. Li and W. Q. Yang, *Nano Energy*, 2024, **120**, 109147.
23. M. S. Zhang, S. Jiang, J. Y. Zou, X. J. Qu, Z. T. Zhang, R. W. Wang and S. L. Qiu, *Acs Appl Nano Mater*, 2023, **6**, 8279-8289.
24. L. Q. Zhang, Y. J. Zhang, S. H. Jiao, J. L. Zhang, X. Zhao, H. L. Chen and J. C. Jiang, *Chemsuschem*, 2023, **16**, e202202393.
25. J. Dai, L. Luo, Z. Tang, Y. Lv, H. Xie, H. Zuo, C. Yang, X. Wang, M. Fan, Y. Xu and L. Dai, *Compos Sci Technol*, 2022, **219**, 109240.
26. J. Dai, X. Qi, L. Xia, Q. Xue, L. Luo, X. Wang, C. Yang, D. Li, H. Xie, A. Cabot, L. Dai and Y. Xu, *Adv Funct Mater*, 2022, **33**, 2212440.
27. G. Zeng, Q. Sun, S. Horta, S. Wang, X. Lu, C. Y. Zhang, J. Li, J. Li, L. Ci, Y. Tian, M. Ibáñez and A. Cabot, *Adv Mater*, 2023, **36**, 2305128.
28. Z. H. Zhang, S. S. Sun, Z. H. Xu and S. G. Yin, *Small*, 2023, **19**, 2302479.
29. A. M. Ghadimi, S. Ghasemi, A. Omrani and F. Mousavi, *Energ Fuel*, 2023, **37**, 3121-3133.
30. F. Mashkoor, M. Shoeb, R. Mashkoor, A. H. Anwer, S. S. Zhu, H. Jeong, S. S. Baek, J. Y. Jung and C. Jeong, *J Clean Prod*, 2023, **418**, 138067.
31. Z. M. Konz, B. M. Wirtz, A. Verma, T.-Y. Huang, H. K. Bergstrom, M. J. Crafton, D. E. Brown, E. J. McShane,

A. M. Colclasure and B. D. McCloskey, *Nature Energy*, 2023, **8**, 450-461.
32. M. Yang, X. Chang, L. Wang, X. Wang, M. Gu, H. Huang, L. Tang, Y. Zhong and H. Xia, *Adv Mater*, 2023, **35**, e2208705.
33. J. Long, S. Tan, J. Wang, F. Xiong, L. Cui, Q. An and L. Mai, *Angew Chem Int Ed Engl*, 2023, **62**, e202301934.
34. S. Zhang, F. Sun, X. Du, X. Zhang, L. Huang, J. Ma, S. Dong, A. Hilger, I. Manke, L. Li, B. Xie, J. Li, Z. Hu, A. C. Komarek, H.-J. Lin, C.-Y. Kuo, C.-T. Chen, P. Han, G. Xu, Z. Cui and G. Cui, *Energy & Environmental Science*, 2023, **16**, 2591-2602.
35. K. L. Ng, B. Amrithraj and G. Azimi, *Joule*, 2022, **6**, 134-170.
36. Z. L. Xu, J. Park, J. Wang, H. Moon, G. Yoon, J. Lim, Y. J. Ko, S. P. Cho, S. Y. Lee and K. Kang, *Nat Commun*, 2021, **12**, 3369.
37. G.-Z. Yang, Y.-F. Chen, B.-Q. Feng, C.-X. Ye, X.-B. Ye, H. Jin, E. Zhou, X. Zeng, Z.-L. Zheng, X.-L. Chen, D.-S. Bin and A.-M. Cao, *Energy & Environmental Science*, 2023, **16**, 1540-1547.
38. Y.-M. Li, Z.-W. Wang, W.-H. Li, X.-Y. Zhang, C. Yin, K. Li, W. Guo, J.-P. Zhang and X.-L. Wu, *Energy Storage Materials*, 2023, **61**, 102873.
39. Y. Huang, M. M. Gao, Y. B. Fu, J. K. Li, F. X. Wang, S. Yang, M. C. Wang, Z. F. Qian, X. Lu, P. P. Zhang and R. H. Wang, *Energy Storage Mater*, 2024, **70**, 103522.
40. P. P. Zhang, M. C. Wang, Y. N. Liu, S. Yang, F. X. Wang, Y. Li, G. B. Chen, Z. C. Li, G. Wang, M. S. Zhu, R. H. Dong, M. H. Yu, O. G. Schmidt and X. L. Feng, *J Am Chem Soc*, 2021, **143**, 10168-10176.
41. P. P. Zhang, Y. Li, G. Wang, F. X. Wang, S. Yang, F. Zhu, X. D. Zhuang, O. G. Schmidt and X. L. Feng, *Adv Mater*, 2019, **31**, 1806005.
42. P. P. Zhang, F. X. Wang, M. H. Yu, X. D. Zhuang and X. L. Feng, *Chem Soc Rev*, 2018, **47**, 7426-7451.
43. G. H. An, J. Hong, S. Pak, Y. Cho, S. Lee, B. Hou and S. Cha, *Adv Energy Mater*, 2019, **10**,1902981.
44. S. Wu, Y. Chen, T. Jiao, J. Zhou, J. Cheng, B. Liu, S. Yang, K. Zhang and W. Zhang, *Adv Energy Mater*, 2019, **9**, 1902915.
45. H. Zhang, Q. Liu, Y. Fang, C. Teng, X. Liu, P. Fang, Y. Tong and X. Lu, *Adv Mater*, 2019, **31**, 1904948.
46. P. A. K. Reddy, H. Y. G. Han, K. C. Kim and S. Bae, *Chem Eng J*, 2023, **471**, 144608.
47. A. M. Zardkhoshoui, B. Ameri and S. S. H. Davarani, *Chem Eng J*, 2023, **470**, 144132.
48. M. R. Thalji, G. A. M. Ali, J. J. Shim and K. F. Chong, *Chem Eng J*, 2023, **473**, 145341.
49. W. W. Liu, J. L. Cheong, M. F. Ng and J. Y. Ying, *Nano Energy*, 2023, **112**, 108489.
50. E. Senokos, D. B. Anthony, N. Rubio, M. C. Ribadeneyra, E. S. Greenhalgh and M. S. P. Shaffer, *Adv Funct Mater*, 2023, **33**, 2212697.
51. M. Gao, Z. Wang, Z. Liu, Y. Huang, F. Wang, M. Wang, S. Yang, J. Li, J. Liu, H. Qi, P. Zhang, X. Lu and X. Feng, *Adv Mater*, 2023, **35**, 2305575
52. S. G. Krishnan, H. D. Pham, C. Padwal, H. Weerathunga, X. J. Wang, K. Mahale and D. Dubal, *J Power Sources*, 2023, **570**, 232994.
53. Y. Wang and S. F. Kuchena, *ACS Omega*, 2022, **7**, 33732-33748.
54. S. N. Zhang, K. Zhu, Y. Y. Gao and D. X. Cao, *Acs Energy Letters*, 2023, **8**, 889-897
55. Y. P. Pan, L. X. Yuan, L. L. Liu, W. W. Fang, Y. Y. Hou, L. J. Fu and Y. P. Wu, *Small Struct*, 2023, **4**, 2300201.
56. X. Y. Zhang, H. Wei, B. H. Ren, J. J. Jiang, G. M. Qu, J. L. Yang, G. M. Chen, H. F. Li, C. Y. Zhi and Z. X. Liu, *Adv Mater*, 2023, **35**. 2304209.
57. D. D. Ling, Q. Wang, G. F. Tian, H. Yu, D. H. Zhang and Q. F. Wang, *Acs Nano*, 2023, **17**, 25222-25233.
58. H. Hong, J. X. Zhu, Y. Q. Wang, Z. Q. Wei, X. Guo, S. Yang, R. Zhang, H. L. Cui, Q. Li, D. C. Zhang and C. Y. Zhi, *Adv Mater*, 2024, **36**, 2308210.
59. H. Chang, X. Y. Liu, S. Zhao, Z. L. Liu, R. T. Lv, Q. Y. Zhang and T. F. Yi, *Adv Funct Mater*, 2024, **34**, 2313491.

60. R. Zhang, S. Wang, S. Chou and H. Jin, *Adv Funct Mater*, 2022, **32**, 2112179.
61. R. Mohanty, U. A. Mohanty and K. Parida, *Energ Fuel*, 2024, **38**, 13585-13611.
62. Y. L. Shao, M. F. El-Kady, J. Y. Sun, Y. G. Li, Q. H. Zhang, M. F. Zhu, H. Z. Wang, B. Dunn and R. B. Kaner, *Chem Rev*, 2018, **118**, 9233-9280.
63. N. Choudhary, C. Li, J. Moore, N. Nagaiah, L. Zhai, Y. Jung and J. Thomas, *Adv Mater*, 2017, **29**, 1605336.
64. V. Sedajová, A. Bakandritsos, P. Blonski, M. Medved, R. Langer, D. Zaoralová, J. Ugolotti, J. Dzíbelová, P. Jakubec, V. Kupka and M. Otyepka, *Energy & Environmental Science*, 2022, **15**, 740-748.
65. C. Knight and G. A. Voth, *Accounts Chem Res*, 2012, **45**, 101-109.
66. D. Marx, A. Chandra and M. E. Tuckerman, *Chem Rev*, 2010, **110**, 2174-2216.
67. T. P. Silverstein, *J Chem Educ*, 2014, **91**, 608-610.
68. L. Yan, J. Huang, Z. Guo, X. Dong, Z. Wang and Y. Wang, *ACS Energy Letters*, 2020, **5**, 685-691.
69. C. Zhong, Y. Deng, W. Hu, J. Qiao, L. Zhang and J. Zhang, *Chemical Society Reviews*, 2015, **44**, 7484-7539.
70. S. Gu, Y. Haoyi, Y. Yuan, Y. Gao, N. Zhu, F. Wu, Y. Bai and C. Wu, *Energy Material Advances*, 2022, **2022**.
71. G. H. Chen, J. Liu, S. L. Ma, C. K. Zhou, J. T. Jiang, Z. Shen, L. J. Yan, Y. Guo, L. J. Yang, Q. Wu, X. Z. Wang and Z. Hu, *Mater Horiz*, 2023, **10**, 5898-5906.
72. W. C. Zhang, Y. J. Liu and Z. P. Guo, *Sci Adv*, 2019, **5,** eaav7412.
73. T. Hosaka, K. Kubota, A. S. Hameed and S. Komaba, *Chem Rev*, 2020, **120**, 6358-6466.
74. J. By E. R. Nightingale, *J. Phys. Chem.*, 1959, **63**, 1381–1387.
75. S. Dong, W. Shin, H. Jiang, X. Wu, Z. Li, J. Holoubek, W. F. Stickle, B. Key, C. Liu, J. Lu, P. A. Greaney, X. Zhang and X. Ji, *Chem*, 2019, **5**, 1537-1551.
76. R. Zheng, Y. Li, H. Yu, X. Zhang, Y. Ding, L. Yan, Y. Li, J. Shu and B. L. Su, *Angew Chem Int Ed Engl*, 2023, **62**, e202301629.
77. J. Han, M. Zarrabeitia, A. Mariani, M. Kuenzel, A. Mullaliu, A. Varzi and S. Passerini, *Adv Mater*, 2022, **34**.
78. K. Itaya, T. Ataka and S. Toshima, *J Am Chem Soc*, 1982, **104**, 4767-4772.
79. C. D. Wessells, S. V. Peddada, M. T. McDowell, R. A. Huggins and Y. Cui, *J Electrochem Soc*, 2012, **159**, A98-A103.
80. X. Y. Wu, Y. T. Qi, J. J. Hong, Z. F. Li, A. S. Hernandez and X. L. Ji, *Angew Chem Int Edit*, 2017, **56**, 13026-13030.
81. Q. Chen, J. Jin, M. Song, X. Zhang, H. Li, J. Zhang, G. Hou, Y. Tang, L. Mai and L. Zhou, *Adv Mater*, 2022, **34**, e2107992.
82. M. Sufyan Javed, X. Zhang, S. Ali, S. Shoaib Ahmad Shah, A. Ahmad, I. Hussain, S. Hussain, K. Shaukat, M. Ouladsmane, S. M. Tag ElDin, W. U. Arifeen and W. Han, *Chem Eng J*, 2023, **471**, 144486.
83. L. Han, J. Luo, R. Zhang, W. Gong, L. Chen, F. Liu, Y. Ling, Y. Dong, Z. Yong, Y. Zhang, L. Wei, X. Zhang, Q. Zhang and Q. Li, *Acs Nano*, 2022, **16**, 14951-14962.
84. Q. Chen, M. Song, X. Zhang, J. Zhang, G. Hou and Y. Tang, *J Mater Chem A*, 2022, **10**, 15614-15622.
85. L. Y. Du, S. S. Bi, M. Yang, Z. W. Tie, M. H. Zhang and Z. Q. Niu, *P Natl Acad Sci USA*, 2022, **119**, e2214545119.
86. Y. Z. Zhang, J. Liang, Z. Huang, Q. Wang, G. Zhu, S. Dong, H. Liang and X. Dong, *Advanced Science*, 2022, **9**, 2105158.
87. J. G. Dai, C. Y. Yang, Y. T. Xu, X. H. Wang, S. Y. Yang, D. X. Li, L. L. Luo, L. Xia, J. S. Li, X. Q. Qi, A. Cabot and L. Z. Dai, *Adv Mater*, 2023, **35**, 2303732.
88. L. T. Ma, H. L. Cui, S. M. Chen, X. L. Li, B. B. Dong and C. Y. Zhi, *Nano Energy*, 2021, **81**, 105632.
89. C. W. Xu, Z. W. Yang, X. K. Zhang, M. T. Xia, H. H. Yan, J. Li, H. X. Yu, L. Y. Zhang and J. Shu, *Nano-Micro Lett*, 2021, **13,** 166.

90. S. Y. Dong, W. Shin, H. Jiang, X. Y. Wu, Z. F. Li, J. Holoubek, W. F. Stickle, B. Key, C. Liu, J. Lu, P. A. Greaney, X. G. Zhang and X. L. Ji, *Chem*, 2019, **5**, 1537-1551.
91. S. Wang, Z. S. Yuan, X. Zhang, S. S. Bi, Z. Zhou, J. L. Tian, Q. C. Zhang and Z. Q. Niu, *Angew Chem Int Edit*, 2021, **60**, 7056-7060.
92. X. J. Mu, Y. Song, Z. M. Qin, J. M. Meng, Z. H. Wang and X. X. Liu, *Chem Eng J*, 2023, **453**, 139575.
93. D. Yang, Y. Song, M. Y. Zhang, Z. M. Qin, J. Liu and X. X. Liu, *Angew Chem Int Edit*, 2022, **61**, e202207711.
94. Q. Chen, H. Li, X. Lou, J. L. Zhang, G. Y. Hou, J. Lu and Y. P. Tang, *Adv Funct Mater*, 2023, **33**, 2214920.
95. Q. Chen, J. Jin, M. Song, X. Zhang, H. Li, J. Zhang, G. Hou, Y. Tang, L. Mai and L. Zhou, *Adv Mater*, 2022, **34**, 2107992.
96. D. Wang, Z. Sun and X. Han, *Journal of the Taiwan Institute of Chemical Engineers*, 2023, **145**, 104845.
97. S. G. Krishnan, H. D. Pham, C. Padwal, H. Weerathunga, X. Wang, K. Mahale and D. Dubal, *J Power Sources*, 2023, **570**, 232994.
98. Y. Z. Fan, Y. Yu, P. Wang, J. J. Sun, M. J. Hu, J. G. Sun, Y. F. Zhang and C. Huang, *J Colloid Interf Sci*, 2023, **633**, 333-342.
99. M. Sufyan Javed, X. Zhang, S. Ali, S. Shoaib Ahmad Shah, A. Ahmad, I. Hussain, S. Hussain, K. Shaukat, M. Ouladsmane, S. M. Tag ElDin, W. U. Arifeen and W. Han, *Chem Eng J*, 2023, **471**, 144486.
100. L. Han, J. Luo, R. Zhang, W. Gong, L. Chen, F. Liu, Y. Ling, Y. Dong, Z. Yong, Y. Zhang, L. Wei, X. Zhang, Q. Zhang and Q. Li, *Acs Nano*, 2022, **16**, 14951-14962.
101. P. Wang, Y. Zhang, H. Jiang, X. Dong and C. Meng, *Chem Eng J*, 2022, **427**, 131548.
102. X. Wang, H. Mei, P. Chang, M. Zhang, T. Hu, L. Cheng and L. Zhang, *Appl Surf Sci*, 2022, **605**, 154688.
103. X. Y. Chen, Z. Y. Feng, X. Y. Dong, H. M. Jiang, C. G. Meng and Y. F. Zhang, *Susmat*, 2023, **3**, 263-275.
104. X. Chen, P. Wang, Z. Feng, Y. Liu, M. Cui, C. Meng and Y. Zhang, *Advanced Sensor and Energy Materials*, 2022, **1**, 100013.
105. P. W. Xingyu Chen, Ziying Feng, Changgong Meng, Yifu Zhang, *Chem Eng J*, **445**, 136747.
106. P. Wang, Y. F. Zhang, Z. Y. Feng, Y. Y. Liu and C. G. Meng, *J Colloid Interf Sci*, 2022, **606**, 1322-1332.
107. D. Wang, J. Sun and L. Chen, *Chemsuschem*, 2023, **16**, e202300207.
108. Y. Liu, Z. Feng, H. Jiang, X. Dong, C. Meng and Y. Zhang, *Green Energy & Environment*, 2024, **9**, 1171-1182.
109. J. G. Dai, X. Q. Qi, L. Xia, Q. Xue, L. L. Luo, X. H. Wang, C. Y. Yang, D. X. Li, H. M. Xie, A. Cabot, L. Z. Dai and Y. T. Xu, *Adv Funct Mater*, 2023, **33**, 2212440.
110. X. Z. Maoting Xia, Haoxiang Yu, Zhengwei Yang, Shi Chen, Liyuan Zhang, and Y. X. Miao Shui, Jie Shu, *Chem Eng J*, 2021, **421**, 127759.
111. W. Y. Chunyang Li, Shishuo Liang, Peng Wang, Jing Wang, and Y. Z. Lijun Fu, Yuhui Chen, Yuping Wu and Wei Huang, *Nanoscale Horizons*, 2019, **4**, 991--998.
112. X. Zhang, M. S. Javed, S. Ali, A. Ahmad, S. S. A. Shah, I. Hussain, D. Choi, A. M. Tighezza, E. Tag-Eldin, C. Xia, S. Ali and W. Han, *Nano Energy*, 2024, **120**, 109108.
113. M. Gao, Z. Wang, Z. Liu, Y. Huang, F. Wang, M. Wang, S. Yang, J. Li, J. Liu, H. Qi, P. Zhang, X. Lu and X. Feng, *Adv Mater*, 2023, **35**, 2305575.
114. K. C. Seetha Lakshmi, X. Ji, L.-D. Shao, B. Vedhanarayanan and T.-W. Lin, *Appl Surf Sci*, 2022, **577**, 151918.
115. Y. Z. Mingxin Shi, Xianggang Zhou, Yingqi Li, Shanshan Xiao, and R. Y. Shanping Liu, Huaqiao Tan, Yonghui Wang, Yangguang Li, *Chem Eng J*, 2023, **464**, 142600.
116. Q. Chen, H. Li, X. Lou, J. Zhang, G. Hou, J. Lu and Y. Tang, *Adv Funct Mater*, 2023, **33**, 2214920.
117. Q. Chen, J. L. Jin, M. D. Song, X. Y. Zhang, H. Li, J. L. Zhang, G. Y. Hou, Y. P. Tang, L. Q. Mai and L. Zhou, *Adv Mater*, 2022, **34**.
118. S. G. Krishnan, C. Padwal, X. J. Wang, H. D. Pham, S. Aberoumand, N. Motta, K. Ostrikov and D. Dubal, *J*

Mater Chem A, 2024, **12**, 8244-8253.
119. K. C. S. Lakshmi, X. B. Ji, L. D. Shao, B. Vedhanarayanan and T. W. Lin, *Appl Surf Sci*, 2022, **577**, 151918.
120. K. C. S. Lakshmi, X. B. Ji, T. Y. Chen, B. Vedhanarayanan and T. W. Lin, *J Power Sources*, 2021, **511**.
121. X. Y. Chen, P. Wang, Z. Y. Feng, C. G. Meng and Y. F. Zhang, *Chem Eng J*, 2022, **445**, 136747.
122. M. S. Javed, X. F. Zhang, S. Ali, S. S. A. Shah, A. Ahmad, I. Hussain, S. Hussain, S. Khan, M. Ouladsmane, S. M. T. ElDin, W. Ul Arifeen and W. H. Han, *Chem Eng J*, 2023, **471**, 144486.
123. J. G. Dai, X. Q. Qi, L. Xia, Q. Xue, L. L. Luo, X. H. Wang, C. Y. Yang, D. X. Li, H. M. Xie, A. Cabot, L. Z. Dai and Y. T. Xu, *Adv Funct Mater*, 2023, **33**, 2212440.
124. D. W. Wang, J. Q. Sun and L. Chen, *Chemsuschem*, 2023, **16**, e202300207.
125. J. G. Dai, C. Y. Yang, Y. T. Xu, X. H. Wang, S. Y. Yang, D. X. Li, L. L. Luo, L. Xia, J. S. Li, X. Q. Qi, A. Cabot and L. Z. Dai, *Adv Mater*, 2023, **35**, 2303732.
126. M. S. Javed, S. S. A. Shah, T. Najam, S. H. Siyal, S. Hussain, M. Saleem, Z. J. Zhao and W. J. Mai, *Nano Energy*, 2020, **77**.
127. P. Wang, Y. F. Zhang, H. M. Jiang, X. Y. Dong and C. G. Meng, *Chem Eng J*, 2022, **427**, 131548.
128. M. Sang, J. J. Wang, D. Y. Zuo, J. Xu, H. W. Zhang and H. J. Li, *Acs Sustain Chem Eng*, 2024, **12**, 2455-2464.
129. X. F. Zhang, M. S. Javed, S. Ali, A. Ahmad, S. S. A. Shah, I. Hussain, D. Choi, A. M. Tighezza, E. Tag-Eldin, C. L. Xia, S. Ali and W. H. Han, *Nano Energy*, 2024, **120**, 109108.
130. S. J. Marje, H. B. Tyagaraj, S. K. Hwang, K. S. Ranjith, E. Alhajri, N. R. Chodankar, Y. S. Huh and Y. K. Han, *J Mater Chem A*, 2024, **12**, 7587-7597.
131. Q. F. Wu, Y. H. Zhang, G. Liu, X. S. Cui, S. Q. Tao, H. Q. Jiang, Y. Lin, R. Peng, X. F. Zhang, Z. Y. Huang, Y. Song, Y. Ding, S. M. Akhlaq, Y. Wu, K. Tao, E. R. Xie, Z. X. Zhang and Z. S. Wu, *Energy Storage Mater*, 2024, **70**, 103474.
132. J. Dai, C. Yang, Y. Xu, X. Wang, S. Yang, D. Li, L. Luo, L. Xia, J. Li, X. Qi, A. Cabot and L. Dai, *Adv Mater*, 2023, **35**, 2303732.
133. H. M. Xiao Wang , Peng Chang , Minggang Zhang , Taotao Hu , Laifei Cheng , Litong Zhang, 2022, **605**, 154688.
134. P. Wang, Y. Zhang, Z. Feng, Y. Liu and C. Meng, *J Colloid Interface Sci*, 2022, **606**, 1322-1332.
135. X. Chen, P. Wang, Z. Feng, C. Meng and Y. Zhang, *Chem Eng J*, 2022, **445**, 136747.
136. X. Chen, Z. Feng, X. Dong, H. Jiang, C. Meng and Y. Zhang, *SusMat*, 2023, **3**, 263-275.
137. Y. Liu, Z. Feng, H. Jiang, X. Dong, C. Meng and Y. Zhang, *Green Energy & Environment*, 2023, 9, 1171-1182.
138. Y. Fan, Y. Yu, P. Wang, J. Sun, M. Hu, J. Sun, Y. Zhang and C. Huang, *J Colloid Interface Sci*, 2023, **633**, 333-342.
139. D. Wang, J. Sun and L. Chen, *ChemSusChem*, 2023, **16**, e202300207.
140. K. C. Seetha Lakshmi, X. Ji, L.-D. Shao, B. Vedhanarayanan and T.-W. Lin, *Appl Surf Sci*, 2022, **577**, 151918.